ELSEVIER

Neutrino oscillation observables from mass matrix structure

Walter Winter

Institut für theoretische Physik und Astrophysik, Universität Würzburg, D-97074 Würzburg, Germany

Abstract

We present a systematic procedure to establish a connection between complex neutrino mass matrix textures and experimental observables, including the Dirac CP phase. In addition, we illustrate how future experimental measurements affect the selection of textures in the $(\theta_{13}, \delta_{CP})$-plane. For the mixing angles, we use generic assumptions motivated by quark–lepton complementarity. We allow for any combination between U_ℓ and U_ν, as well as we average over all present complex phases. We find that individual textures lead to very different distributions of the observables, such as to large or small leptonic CP violation. In addition, we find that the extended quark–lepton complementarity approach motivates future precision measurements of δ_{CP} at the level of $\theta_C \simeq 11°$.
© 2007 Elsevier B.V. Open access under CC BY license.

1. Introduction

By using the same parameterization for V_{CKM} and U_{PMNS}, and by quantifying the differences between these two mixing matrices, it is implied that the quark and lepton sectors might be somehow connected. Recently, interesting "quark–lepton complementarity" (QLC) relations [1–4] have been proposed, which could be indicative for such a quark–lepton unification. These QLC relations suggest empirical connections between quark and lepton mixings, such as

$$\theta_{12} + \theta_C \simeq \pi/4 \simeq \theta_{23}. \tag{1}$$

A simple underlying hypothesis may therefore be that all mixings in the charged lepton and neutrino sectors are either maximal, or Cabibbo-like. It can be motivated by the observation that mixing angles $\sim \theta_C$ (and powers $\sim \theta_C^n$ thereof), as well as maximal mixing, can be readily obtained in models from flavor symmetries. Consequently, any deviation from maximal mixing in the large leptonic mixing angles θ_{12} and θ_{23} can only arise as a result of taking the product of the charged lepton mixing ma-

trix U_ℓ and the neutrino mixing matrix U_ν in the PMNS mixing matrix

$$U_{PMNS} = U_\ell^\dagger U_\nu. \tag{2}$$

If one assumes that all mixing angles in U_ℓ and U_ν can only be from the sequence $\{\pi/4, 0, \epsilon, \epsilon^2, \ldots\}$ with $\epsilon \simeq \theta_C$, one can systematically construct the parameter space of all possible combinations of U_ℓ and U_ν in this framework and choose the realizations being compatible with data. This analysis was performed in Ref. [5] for the case of real matrices up to oder ϵ^2, and it was called "extended quark–lepton complementarity" (for a seesaw implementation, see Ref. [6]). Simple conventional quark–lepton complementarity implementations, such as $U_{PMNS} \simeq V_{CKM}^\dagger U_{bimax}$, emerge as special cases in this approach (see, e.g., Refs. [7,8]), but are not the exclusive solutions. For example, the charged lepton sector may actually induce two large mixing angles.

Any realization of Eq. (2) can be used to construct the effective Majorana neutrino mass matrix as

$$M_\nu^{Maj} = U_\nu M_\nu^{diag} U_\nu^T, \tag{3}$$

where we can use the experimentally motivated mass eigenvalues, such as $m_1 : m_2 : m_3 \simeq \epsilon^2 : \epsilon : 1$ for the normal hierarchy.

E-mail address: winter@physik.uni-wuerzburg.de.

This additional assumption for the neutrino mass eigenvalues is compatible with the current measurements of Δm_{21}^2 and Δm_{31}^2. Similarly, the charged lepton and quark mass hierarchies can be described by powers of ϵ as well, which means that by our hypothesis, all mixings and hierarchies are induced by a single small quantity $\epsilon \simeq \theta_C$ as a potential remnant of a unified theory. By identifying the leading order entries in the mass matrix realization Eq. (3), the "texture", one can establish a connection to theoretical models. For example, masses for quarks and leptons may arise from higher-dimension terms via the Froggatt–Nielsen mechanism [9] in combination with a flavor symmetry:

$$\mathcal{L}_{\text{eff}} \sim \langle H \rangle \epsilon^n \bar{\Psi}_L \Psi_R. \tag{4}$$

In this case, ϵ becomes meaningful in terms of a small parameter $\epsilon = v/M_F$ which controls the flavor symmetry breaking.[1] The integer power of ϵ is solely determined by the quantum numbers of the fermions under the flavor symmetry (see, e.g., Refs. [6,10]).

In this Letter, we demonstrate how one can construct the full *complex* parameter space of realizations of Eq. (2) from generic assumptions. We use the context of extended quark–lepton complementarity to illustrate our procedure, where we average over all possible complex phases. Since we will obtain a $1:n$ correspondence between a texture and a number of valid (experimentally allowed) realizations of this texture, we can study the distributions of observables corresponding to the realizations. We will focus on the effective Majorana neutrino mass matrix for the normal hierarchy, but this procedure can easily be extended to the neutrino Dirac mass matrix and charged lepton mass matrix, as well as one can use different neutrino mass schemes [5], or different generic input assumptions.

2. Method

Following the procedure in Ref. [5], the PMNS matrix can, in general, be written as the product of two matrices in the CKM-like standard parameterization $\hat{U}$:

$$U_{\text{PMNS}} = \hat{U}_\ell^\dagger U_\nu = \hat{U}_\ell^\dagger D \hat{U}_\nu K. \tag{5}$$

Here $D = \text{diag}(1, e^{i\varphi_1}, e^{i\varphi_2})$ and $K = \text{diag}(e^{i\phi_1}, e^{i\phi_2}, 1)$ are remaining diagonal matrices with phases in the range $\varphi_1, \varphi_2, \phi_1, \phi_2 \in [0, 2\pi)$, which cannot be rotated away in general because of the CKM-like parameterizations of $\hat{U}_\ell$ and $\hat{U}_\nu$. In addition, $\hat{U}_\alpha$ can be parameterized by three mixing angles θ_{12}^α, θ_{13}^α, and θ_{23}^α, as well as one Dirac-like phase δ^α in the usual way. Our three-step procedure then reads:

Step 1. We generate all possible pairs $\{U_\ell, U_\nu\}$ described by

$$\{\theta_{12}^\ell, \theta_{13}^\ell, \theta_{23}^\ell, \delta^\ell, \theta_{12}^\nu, \theta_{13}^\nu, \theta_{23}^\nu, \delta^\nu, \varphi_1, \varphi_2, \phi_1, \phi_2\},$$

with $\sin\theta_{ij}^\alpha \in \{1/\sqrt{2}, \epsilon, \epsilon^2, 0\}$ (cut off by the current experimental precision) and uniform distributions of all phases in 32 steps each, which corresponds to an averaging over the phases.[2]

Step 2. Then we calculate U_{PMNS} by Eq. (2), read off the mixing angles and physical phases, and select those *realizations* with mixing angles being compatible with current data at the 3σ confidence level (cf., Ref. [5]).

Step 3. For each valid realization, we find the corresponding *texture* by computing Eq. (3), expanding in ϵ, and by identifying the first non-vanishing coefficient, which is leading to the texture entry 1, ϵ, ϵ^2, or 0.[3]

Obviously, many possible realizations will lead to the same texture, i.e., there will be a $1:n$ correspondence between textures and realizations. We will therefore show the distributions of observables for all valid realizations (valid choices of order one coefficients) leading to a specific texture. The interpretation of the results has then to be done in the reverse direction: A certain model will lead to a specific texture, which can be fit to data by choosing the order one coefficients from our set of realizations. Note that the realizations connect to experimental observations, while the textures connect to theoretical models.

3. Results and interpretation

We find 29 different textures for M_ν^{Maj} from the above procedure. These come from realizations which represent valid choices of U_{PMNS}. In Table 1, we show seven selected textures (see Ref. [11] for a complete list and examples of corresponding M_ℓ textures computed as in Ref. [5]). The percentage of all realizations leading to a specific texture is given in the third column. The distributions of the observables $\sin^2 2\theta_{13}$, δ, $\sin^2 \theta_{12}$ and $\sin^2 \theta_{23}$ are given in the last column (arbitrary units), where the current best-fit values are marked by vertical lines. In Table 2, we give specific examples for realizations leading to a specific texture, where we have chosen cases with $\sin^2 \theta_{12}$ and $\sin^2 \theta_{23}$ very close to the current best-fit values. One can read off this table valid combinations between U_ℓ and U_ν leading to specific textures referred to by the texture number. For example, only the shown realizations leading to textures #1 and #7 have exclusively small mixings coming from the lepton sector. The choice $\phi_1 = \phi_2 = 0$ in this table is accidental (it does not appear for more seldom textures). In comparison to Ref. [5], we focus on M_ν^{Maj}, and we obtain a much larger number of textures for M_ν^{Maj}. Allowing for the current measurement errors instead of the more stringent ones used in Ref. [5], 13 more textures in addition to the 6 original ones are allowed. If, in addition, complex phases are introduced instead of using the real case only, we find 10 more textures, leading to a total of 29 (cf. Ref. [11] for details on which textures are falling into which category).

---

[1] Here v are universal VEVs of SM singlet scalar "flavons" that break the flavor symmetry, and M_F refers to the mass of superheavy fermions, which are charged under the flavor symmetry. The SM fermions are given by the Ψ's.

[2] We have checked that 32 steps are sufficient to reproduce the general qualitative features.

[3] Note that this definition of a texture only includes the absolute value of the leading coefficient, while more sophisticated concepts may include the phase as well.

Table 1
Selected textures for M_ν^{Maj}. "Percentage" refers to the fraction of all realizations leading to a texture

No.	Texture	Percentage	Distributions of valid realizations leading to this texture
#1	$\begin{pmatrix} \epsilon & \epsilon & \epsilon \\ \epsilon & 1 & 1 \\ \epsilon & 1 & 1 \end{pmatrix}$	41%	
#2	$\begin{pmatrix} \epsilon & \epsilon & \epsilon^2 \\ \epsilon & \epsilon & \epsilon \\ \epsilon^2 & \epsilon & 1 \end{pmatrix}$	8.4%	
#3	$\begin{pmatrix} \epsilon & \epsilon & 0 \\ \epsilon & \epsilon & 0 \\ 0 & 0 & 1 \end{pmatrix}$	5.6%	
#4	$\begin{pmatrix} 1 & \epsilon^2 & 1 \\ \epsilon^2 & \epsilon & \epsilon^2 \\ 1 & \epsilon^2 & 1 \end{pmatrix}$	5.4%	
#5	$\begin{pmatrix} \epsilon & \epsilon & \epsilon \\ \epsilon & \epsilon & \epsilon^2 \\ \epsilon & \epsilon^2 & 1 \end{pmatrix}$	4.8%	
#6	$\begin{pmatrix} 1 & 0 & 1 \\ 0 & \epsilon & 0 \\ 1 & 0 & 1 \end{pmatrix}$	1.4%	
#7	$\begin{pmatrix} \epsilon^2 & \epsilon^2 & \epsilon^2 \\ \epsilon^2 & 1 & 1 \\ \epsilon^2 & 1 & 1 \end{pmatrix}$	0.5%	

Table 2
Examples for specific realizations for the textures in Table 1 (including the mixings from the lepton sector). All of the shown realizations have observables very close to the current best-fit values

Text. No.	Observables $(\sin^2\theta_{12}, \sin^2 2\theta_{13}, \sin^2\theta_{23}, \delta)$	Input parameters		
		$(s_{12}^\ell, s_{13}^\ell, s_{23}^\ell, \delta^\ell)$	$(s_{12}^\nu, s_{13}^\nu, s_{23}^\nu, \delta^\nu)$	$(\varphi_1, \varphi_2, \phi_1, \phi_2)$
#1	$(0.30, 0.15, 0.50, 4.70)$	$(\epsilon, \epsilon, \epsilon^2, 5.30)$	$(\frac{1}{\sqrt{2}}, \epsilon, \frac{1}{\sqrt{2}}, 4.71)$	$(5.50, 1.37, 0, 0)$
#2	$(0.30, 0.15, 0.50, 4.74)$	$(\epsilon, \epsilon, \frac{1}{\sqrt{2}}, 4.32)$	$(\frac{1}{\sqrt{2}}, 0, \epsilon, 0)$	$(5.30, 0.59, 0, 0)$
#3	$(0.30, 0.15, 0.50, 4.74)$	$(\epsilon, \epsilon, \frac{1}{\sqrt{2}}, 4.71)$	$(\frac{1}{\sqrt{2}}, 0, 0, 0)$	$(5.50, 2.55, 0, 0)$
#4	$(0.30, 0.01, 0.50, 2.61)$	$(\frac{1}{\sqrt{2}}, \frac{1}{\sqrt{2}}, \frac{1}{\sqrt{2}}, 4.91)$	$(\epsilon, \frac{1}{\sqrt{2}}, \epsilon^2, 0.20)$	$(0.20, 3.53, 0, 0)$
#5	$(0.30, 0.05, 0.50, 4.89)$	$(\epsilon, \epsilon, \frac{1}{\sqrt{2}}, 0.59)$	$(\frac{1}{\sqrt{2}}, \epsilon, \epsilon^2, 0.39)$	$(5.89, 1.18, 0, 0)$
#6	$(0.32, 0.13, 0.47, 3.57)$	$(\frac{1}{\sqrt{2}}, \frac{1}{\sqrt{2}}, \frac{1}{\sqrt{2}}, 1.77)$	$(0, \frac{1}{\sqrt{2}}, 0, 3.53)$	$(0, 5.69, 0, 0)$
#7	$(0.22, 0.01, 0.50, 3.18)$	$(\epsilon, \epsilon, \epsilon^2, 2.55)$	$(\epsilon, \epsilon^2, \frac{1}{\sqrt{2}}, 3.14)$	$(3.14, 2.55, 0, 0)$

As far as the interpretation of the distributions of the observables in Table 1 is concerned, it certainly depends on the measure of the input parameter space, in particular, our choice of discrete values for the mixing angles. Our choice $\propto \epsilon^n$ corresponds to a uniform (anarchic) distribution on a logarithmic scale. At the mass matrix level, one may justify such an assumption by the Froggatt–Nielsen mechanism by using an arbitrary number of heavy fermion propagators in Eq. (4). The quark and lepton mass hierarchies seem to obey such a "logarithmic uniformity" as well, which means that this assumption may be well motivated for the eigenvalues. Our choices for the mixing angles correspond to the postulate that we find, at least roughly, this distribution in the matrix elements reflected in the mixing angles. We have therefore checked that our distribution of mixing angles translates into a similar (uniform) distribution of mass matrix powers if one allows for all possible hierarchies. In fact, there is a slight (but not order of magnitude-wise) deviation from this uniformity for the diagonal elements leading to a peak at 1, and for the off-diagonal elements leading to a peak at ϵ^2. The choice of a normal neutrino mass hierarchy is an additional, experimentally motivated constraint, which obviously affects the mapping between the mass matrix and mixing angle parameter spaces.

Given our assumptions for the input values, the interpretation of our figures is then as follows from the experimental point of view: For the valleys where no realizations are found, a measurement could exclude a texture. For the peaks, where most realizations are found, a measurement would confirm the most "natural" choice of observables. This naturalness argument may be similar to a landscape interpretation, such as in Refs. [12,13] (using a different measure). Note, however, that we impose at least some flavor structure before we obtain the distributions. Similarly, the figures can be interpreted from the model building point of view: The peaks correspond to plenty of possibilities how a specific texture can be implemented. For the valleys, where only a few realizations are found, exceptional realizations can lead to this texture. This means that one can basically read off such tables which textures to use if one wants to produce small $\sin^2 2\theta_{13}$, large $\sin^2 2\theta_{13}$, deviations from maximal mixing, etc.

We discuss now the different observables. For $\sin^2\theta_{23}$, either maximal mixing, or relatively large deviations from maximal mixing can be observed. Only texture #2 has a relatively broad distribution in this observable. Deviations from maximal mixing will therefore be an important model discriminator, see Ref. [14]. For $\sin^2\theta_{12}$, the current best-fit value can only be exactly generated in very few cases, which is not surprising since θ_{12} has to emerge from combinations between maximal mixing and θ_C in our approach. Only texture #4 covers the current best-fit value very well. Therefore, precise measurements of $\sin^2\theta_{12}$ will be very valuable for such a quark–lepton complementarity ansatz. For $\sin^2 2\theta_{13}$, any case can be found: large $\sin^2 2\theta_{13}$ (e.g., #4), small $\sin^2 2\theta_{13}$ (e.g., #7), medium $\sin^2 2\theta_{13}$ (e.g., #1), or a broad distribution in $\sin^2 2\theta_{13}$ (e.g., #5). And for δ_{CP}, maximal CP violation (#5 and #7), CP conservation, or small deviations from these cases at the level of $\pi/16 \sim \theta_C$ are present. This can be understood as follows: The phases may be given in the symmetry base of an underlying theory, where uniform distributions (or any other assumptions) may be well motivated. These assumptions translate (via invariants) into the observables, where combinations with the mixing angles enter. Obviously, by choosing powers of the Cabibbo angle for the mixing angles, these powers will somehow translate into the phase distributions. This implies that a measurement precision of $\sim 11°$ may be a reasonable requirement for future experiments to test a small CP violation. Such a precision could be obtained in optimized beta beams or neutrino factories (see, e.g., Ref. [15]).

Let us now discuss the use of simultaneous constraints on $\sin^2 2\theta_{13}$ and δ_{CP} on this texture space. We show in Fig. 1, left, clusters representing 50% of all valid realizations for different selected textures in the $\sin^2 2\theta_{13}$-δ_{CP}-plane. In Fig. 1, right, we show the precision for a typical potential future high precision instrument, namely the $\gamma = 350$ beta beam option from Ref. [16] simulated with GLoBES [17,18].[4] From Fig. 1,

---

[4] This setup assumes eight years of simultaneous operation with 2.9×10^{18} useful ^{6}He and 1.1×10^{18} useful ^{18}Ne decays per year and a 500 kt water Cherenkov detector. The gamma factor is 350 for both isotopes, and the baseline is $L = 730$ km. The setups is simulated with the migration matrices from
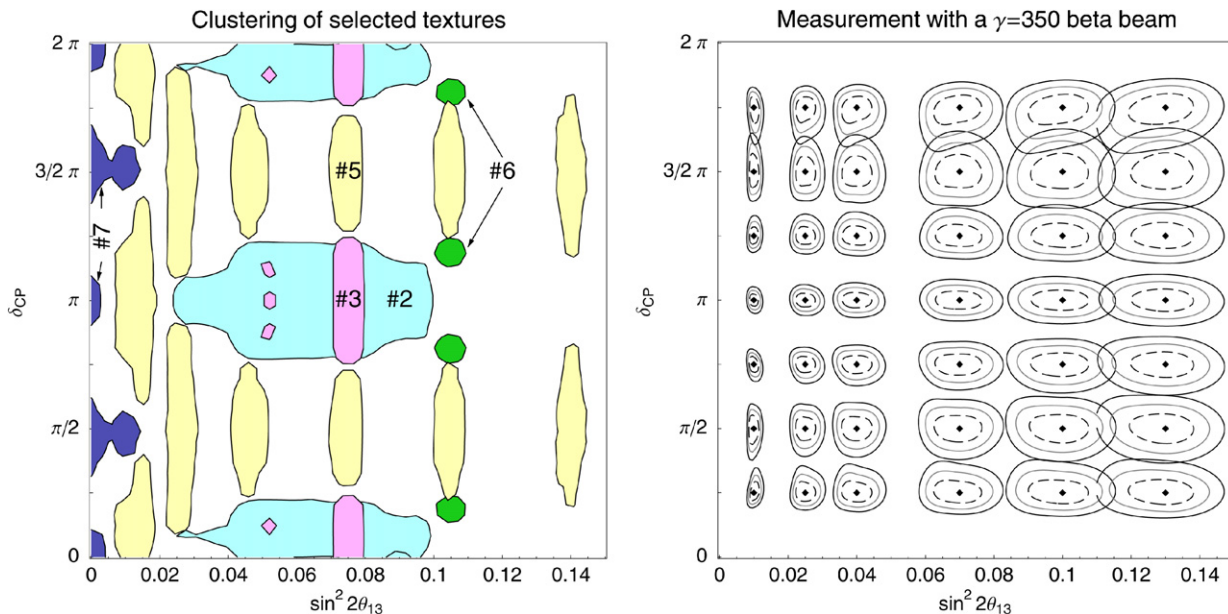
Fig. 1. Left panel: Clustering of specific textures (as labeled in the plot) in the $\sin^2 2\theta_{13}$-δ_{CP}-plane. The clusters contain 50% of all realizations leading to a specific texture. Right panel: Measurement precision of a $\gamma = 350$ beta beam for different selected true values of $\sin^2 2\theta_{13}$ and δ_{CP} (diamonds). The contours correspond to 1σ, 2σ, and 3σ (2 d.o.f., not shown oscillation parameters marginalized over).

left, which represents the two-dimensional version of the histograms in Table 1, we find that the realization distributions for different textures cluster in different, often non-overlapping regions of the $\sin^2 2\theta_{13}$-δ_{CP}-plane. Therefore, in order to distinguish many different textures, combined information on both $\sin^2 2\theta_{13}$ and δ_{CP} is useful. For example, for #5, all possible values of $\sin^2 2\theta_{13}$ and δ_{CP} are covered by the clusters. However, a simultaneous measurement of $\sin^2 2\theta_{13}$ and δ_{CP} (cf. right panel) may easily indicate that this cluster is not realized because certain regions in the $\sin^2 2\theta_{13}$-δ_{CP}-plane are sparsely populated. From the right panel we learn that, compared to the texture cluster sizes, the future experiments will provide very precise measurements in this parameter space. In particular cases, such as for texture #5, a separate measurement of $\sin^2 2\theta_{13}$ or δ_{CP} could hardly exclude the texture, but a combined measurement might (depending on the best-fit point). Therefore, we conclude that a simultaneous measurement of $\sin^2 2\theta_{13}$ and δ_{CP}, as it is usually discussed from the experimental point of view, will be a much stronger discriminator than an individual measurement of one of these parameters.

4. Summary and conclusions

We have demonstrated how one can systematically construct experimentally allowed realizations of U_{PMNS} from very generic assumptions, and we have used them to relate neutrino mass textures with observables. Our procedure can be easily applied to other observables, different (or additional) assumptions, different neutrino mass schemes, or to the Dirac mass matrix case. The resulting distributions of observables could

be useful for experiments, such as to illustrate their exclusion power in the model space, and theorists, such as to identify textures connected with specific distributions for the observables. It turns out the possibilities leading to a specific texture can often be connected with very characteristic observable distributions, such as small $\sin^2 2\theta_{13}$, large $\sin^2 2\theta_{13}$, strong CP violation, CP conservation, a strong deviation from maximal mixing, etc.

As an example, we have used the context of extended quark–lepton complementarity to apply our procedure: All mixing angles are forced to either zero or maximal by a symmetry, or are generated by a quantity $\simeq \theta_C$ as a single remnant from a Grand Unified Theory. This framework means that the solar mixing angle can only emerge as a combination between maximal mixing and the Cabibbo angle, and it is directly related to the quark sector. As more specific conclusions from this assumption, we find that θ_{12} will be an important indicator for specific textures, i.e., future precision measurements of θ_{12} will be very selective. In addition, the extended quark–lepton complementarity ansatz motivates future precision measurements of δ_{CP} at the level of $\pm\theta_C \simeq \pm\pi/16 \simeq 11°$. Such hints are important for the design of future experiments, since one would like to know how far one has to go experimentally.

References

Ref. [16]. In order to impose constraints to the atmospheric parameters, ten years of T2K disappearance information is added (such as in Ref. [19]).

[1] S.T. Petcov, A.Y. Smirnov, Phys. Lett. B 322 (1994) 109, hep-ph/9311204.

[2] A.Y. Smirnov, hep-ph/0402264.
[3] M. Raidal, Phys. Rev. Lett. 93 (2004) 161801, hep-ph/0404046.
[4] H. Minakata, A.Y. Smirnov, Phys. Rev. D 70 (2004) 073009, hep-ph/0405088.
[5] F. Plentinger, G. Seidl, W. Winter, Nucl. Phys. B 791 (2008) 60, hep-ph/0612169.
[6] F. Plentinger, G. Seidl, W. Winter, arXiv: 0707.2379 [hep-ph].
[7] A. Datta, L. Everett, P. Ramond, Phys. Lett. B 620 (2005) 42, hep-ph/0503222.
[8] L.L. Everett, Phys. Rev. D 73 (2006) 013011, hep-ph/0510256.
[9] C.D. Froggatt, H.B. Nielsen, Nucl. Phys. B 147 (1979) 277.
[10] T. Enkhbat, G. Seidl, Nucl. Phys. B 730 (2005) 223, hep-ph/0504104.
[11] W. Winter, Complex texture webpage, http://theorie.physik.uni-wuerzburg.de/~winter/Resources/CTex/index.html.
[12] L.J. Hall, M.P. Salem, T. Watari, arXiv: 0707.3446 [hep-ph].
[13] L.J. Hall, M.P. Salem, T. Watari, arXiv: 0707.3444 [hep-ph].
[14] S. Antusch, et al., Phys. Rev. D 70 (2004) 097302, hep-ph/0404268.
[15] P. Huber, M. Lindner, W. Winter, JHEP 0505 (2005) 020, hep-ph/0412199.
[16] J. Burguet-Castell, et al., Nucl. Phys. B 725 (2005) 306, hep-ph/0503021.
[17] P. Huber, M. Lindner, W. Winter, Comput. Phys. Commun. 167 (2005) 195, hep-ph/0407333.
[18] P. Huber, et al., Comput. Phys. Commun. 177 (2007) 432, hep-ph/0701187.
[19] P. Huber, et al., Phys. Rev. D 73 (2006) 053002, hep-ph/0506237.